High tensile ductility in a nanostructured metal

Yinmin Wang*, Mingwei Chen†, Fenghua Zhou† & En Ma*

** Department of Materials Science and Engineering,*
† Department of Mechanical Engineering, The Johns Hopkins University, Baltimore, Maryland 21218, USA

Nanocrystalline metals—with grain sizes of less than 100 nm—have strengths exceeding those of coarse-grained and even alloyed metals[1,2], and are thus expected to have many applications. For example, pure nanocrystalline Cu (refs 1–7) has a yield strength in excess of 400 MPa, which is six times higher than that of coarse-grained Cu. But nanocrystalline materials often exhibit low tensile ductility at room temperature, which limits their practical utility. The elongation to failure is typically less than a few per cent; the regime of uniform deformation is even smaller[1–7]. Here we describe a thermomechanical treatment of Cu that results in a bimodal grain size distribution, with micrometre-sized grains embedded inside a matrix of nanocrystalline and ultrafine (<300 nm) grains. The matrix grains impart high strength, as expected from an extrapolation of the Hall–Petch relationship. Meanwhile, the inhomogeneous microstructure induces strain hardening mechanisms[8–11] that stabilize the tensile deformation, leading to a high tensile ductility—65% elongation to failure, and 30% uniform elongation. We expect that these results will have implications in the development of tough nanostructured metals for forming operations and high-performance structural applications including microelectromechanical and biomedical systems.

The pure copper used in this model study is very ductile in its annealed and coarse-grained form. It has an elongation to failure as large as 70% (curve A, Fig. 1), but a low yield strength (σ_y). Strengthening through heavy cold work results in a material with a tensile curve that peaks immediately after yielding (curve B, Fig. 1). Such a trend of strengthening accompanied by a loss of ductility is generally true for Cu and other metals processed in various ways[1–7,12], as summarized in Fig. 2.

Our processing starts by rolling the Cu at liquid nitrogen temperature to a high value of percentage cold work (CW; see Methods). The resulting material has a typical heavily deformed microstructure with high densities of dislocations in nanoscale networks[13,14], with some resolvable grains all below 200 nm in size[14]. The use of the low temperature suppresses dynamic recovery, allowing the density of the accumulated dislocations to reach a higher steady-state level than that achievable at room temperature. Transmission electron micrographs of the microstructures after recovery annealing and recrystallization are shown in Fig. 3a, b. The recrystallized grains have well-defined, high-angle boundaries (Fig. 3b). The majority of the grains are in the nanocrystalline to ultrafine range. Meanwhile, abnormal grain growth (secondary recrystallization[15]) has started to produce a volume fraction (~25%) of coarser (1–3 μm) grains, some of which contain annealing twins.

The engineering stress–strain curves corresponding to the microstructures in Fig. 3 are compared in Fig. 1. After 93% CW at liquid-nitrogen temperature (curve C), the σ_y is much higher than that of the room-temperature-rolled Cu (95% CW; curve B). The elongation to failure is also significantly larger. After the 180 °C annealing, the σ_y decreased slightly for the recovered and partially recrystallized grains, and the elongation to failure increased further (curve D). Such concurrent strengthening and toughening (in terms of post-necking elongation), as observed for both curves C and D when compared with curve B, can be attributed to the nanocrystalline/ultrafine grains that reduce the size of nucleating flaws and increase the resistance to crack propagation, leading to a higher fracture stress[1]. Micrographs of the fracture surfaces (not shown) indicate that ductile fracture through the nucleation and coalescence of extremely fine microvoids was promoted[14]. The radial unstable crack growth was delayed, and the stabilizing triaxial stress state was maintained to larger strains[16].

A marked improvement in uniform elongation was found concurrent with pronounced strain hardening, without sacrificing much of the strength, in material with the bimodal microstructure shown in Fig. 3b. The resultant stress–strain curve is shown in Fig. 1 (curve E). The large densities of defects and cold-work energy stored during processing at liquid nitrogen temperature allowed copious nucleation during recrystallization at a low temperature, so that the vast majority of the matrix grains are kept in the nanocrystalline/ultrafine grain regime to help maintain the high strength of the 'composite' material. Meanwhile, the grains with sufficiently large sizes obtained through secondary recrystallization, at a volume fraction of 25%, produced pronounced strain hardening to sustain the useful uniform deformation to large strains. Note that one should not restore strain hardening by allowing uniform growth of all grains or a large fraction of excessively grown grains, both of which would cause an additional unwanted drop in σ_y.

The strain hardening is needed because the onset of localized deformation (necking instability, peak in Fig. 1) in tension is governed by the Considére criterion[17–19]

$$\left(\frac{\partial\sigma}{\partial\varepsilon}\right)_{\dot{\varepsilon}} \leq \sigma \qquad (1)$$

where σ and ε are true stress and true strain, respectively. The nanocrystalline and ultrafine matrix grains tend to lose the work hardening (left-hand side of equation (1)) quickly on deformation owing to their very low dislocation storage efficiency inside the tiny grains, especially when in presence of dynamic recovery[20]. Such a high-strength material is therefore prone to plastic instability (early necking), severely limiting the desirable uniform elongation unless larger grains of appropriate sizes and volume fractions are present.

Our strategy is to efficiently use the moderate population of the larger grains to achieve a strain hardening rate much higher than that which would be expected from curve A (Fig. 1, for uniform deformation under uniaxial tension). We do this by taking advantage of the following three factors. First, these confined grains deformed in the inhomogeneous microstructure are under multi-axial stress states. There are complex strain paths and triaxial

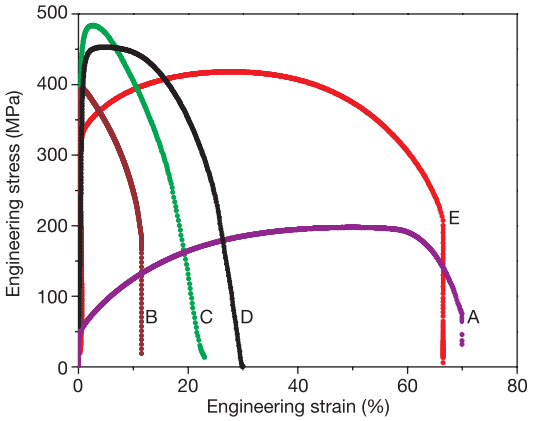

Figure 1 Engineering stress–strain curves for pure Cu. Curve A, annealed, coarse-grained Cu; B, room temperature rolling to 95% cold work (CW); C, liquid-nitrogen-temperature rolling to 93% CW; D, 93% CW + 180 °C, 3 min.; and E, 93% CW + 200 °C, 3 min. Note the coexisting high strength and large uniform plastic strain as well as large overall percentage elongation to failure for curve E.

strain components, with very large strain gradients (see Supplementary Information). It is known that a complex stress state, complicated straining patterns and dislocation configurations, and high densities of geometrically necessary dislocations are all beneficial for promoting grain refinement (or dislocation storage and strain hardening). For example, equal channel angular pressing (ECAP) uses similar conditions to make nanostructured metals in an efficient way[21]. For a metal such as Cu, the non-uniform deformation over a length scale of the order of a few micrometres (Fig. 3b) is the realm of strain-gradient plasticity theory[11], which predicts significant strain hardening owing to an excessively large number of geometrically necessary dislocations that are forced to be present to accommodate the large strain gradient.

Second, $\langle 112 \rangle \{11\bar{1}\}$ twinning, as shown in Fig. 4a and the selected-area electron diffraction pattern in the upper left inset, was observed unexpectedly after straining for 6% inside most of these larger grains. Deformation twins have not been observed for Cu before except at high strain rates or low, sub-ambient temperatures, and activation of such twins is known to require high stresses, especially when the grain sizes are small[8,9,22,23]. Additional observations by transmission electron microscopy (for example, the high-resolution image in Fig. 4a lower right inset) show twin boundaries located preferentially near the protrusions of the surrounding nanocrystalline/ultrafine grains into the softer large grains, suggesting twinning initiation presumably due to stress concentration. The activation of the twinning mechanism suggests that these constrained larger grains plastically deform at high stresses, consistent with the high strength observed. In terms of enhancing strain hardening, twinning is known to be highly effective in conventional Cu (refs 8, 9), owing to dislocation pileups at the twin boundaries (Fig. 4a). In nanocrystalline Cu, the interfaces generated between twinned segments can act as strong barriers to dislocation motion[10].

Third, the larger (softer) grains accommodate strains preferentially (see Supplementary Information). When the overall uniform elongation reached ~30% (peak of curve E in Fig. 1), these larger grains had accumulated large numbers of twin boundaries, dislocations and subgrain boundaries such that the microstructure was refined to a level similar to the nanocrystalline/ultrafine grained matrix, Fig. 4b). Afterwards, the post-necking elongation is similar to that discussed for the sample annealed at 180 °C (curve D in Fig. 1). Overall, the nanostructured Cu of curve E (Fig. 1), when compared with the coarse grained starting material, represents an elevation of σ_y by a factor of 5–6 while maintaining comparable elongation to failure. The simultaneous high strength and ductility, especially the very large uniform deformation at the elevated strength, results in an notable gain in toughness (the area under the stress–strain curve)[16]. This is what sets this material apart from all previous treated copper materials, as demonstrated in Fig. 2.

To establish the reproducibility, three additional samples with or without the ECAP step were processed through similar CW and heat treatment. In all cases, coexisting high strength and ductility were observed. Further annealing beyond that shown in Fig. 3b caused additional grain growth and larger uniform elongation, but with a large decrease in σ_y and no gain in overall ductility owing to the decrease of the post-peak elongation (compare curve A with curve D, Fig. 1). Attempts to start with the room-temperature-rolled Cu only managed a σ_y of ~100 MPa when elongation to failure reached ~50%. This emphasizes the importance of the step at liquid nitrogen temperature, which stores large cold work energy that leads to a lower recrystallization temperature (compared with room-temperature rolling, the calorimetric recrystallization/grain growth peak temperature decreased by 60 °C) and favours copious nucleation over growth. This makes it possible to achieve the

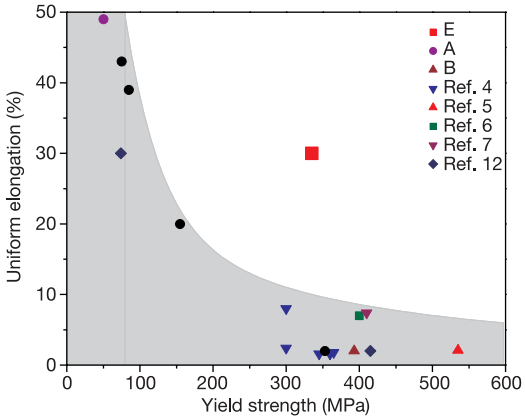

Figure 2 Representative tensile properties of pure Cu. The data are for Cu of conventional, ultrafine and nanocrystalline grain sizes[4–7,12], and after cold rolling to various degrees of CW from our own tests (filled black circles). Data points E, A and B are from the corresponding curves in Fig. 1. Uniform elongation up to the peak in the engineering stress–strain curve is compared here, not only because it is a desirable property but also because the overall percentage elongation to failure is often dominated by localized deformation (necking) whose magnitude depends on the gauge length used in the different experiments. The 'tough Cu' developed here (E) is clearly separated from the general trend.

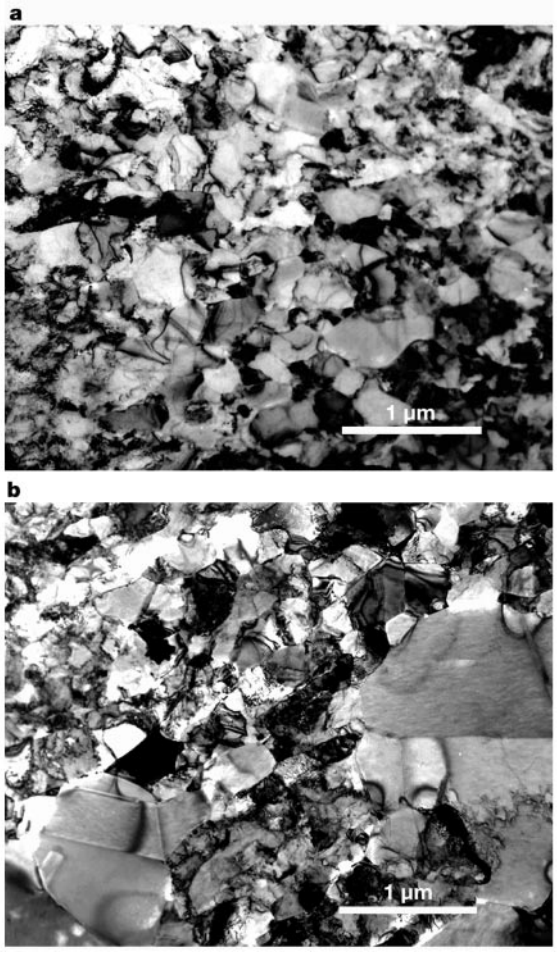

Figure 3 Transmission electron micrographs showing the evolution of the Cu microstructure. Panels **a** and **b** show the samples used to obtain the curves D and E in Fig. 1, respectively. After annealing at 180 °C for 3 min (**a**), recovery has occurred, and the dislocation density is much reduced. The vast majority of the grains are in the nanocrystalline/ultrafine range, with some recrystallized regions. Heat-treating at 200 °C for 3 min led to full recrystallization followed by secondary recrystallization (**b**).

nanocrystalline/ultrafine grained matrix structure through recrystallization, thus affording room for tailoring the microstructure through controlled secondary recrystallization[15].

Our approach does not use uniform nanocrystalline grains, which have to rely on grain boundary deformation mechanisms (such as grain boundary sliding) to contribute significantly to ductility and stabilize the plastic deformation through large increases in strain rate sensitivity[6,24–26]. Experimental data so far (for example, Fig. 2) indicate that at ambient temperature the increase in ductility provided by grain boundary sliding in small grains is either insufficient to compensate for the loss of dislocation controlled ductility, or concurrent with a much reduced strength[2,6].

Our idea of improving strain hardening may be used to derive good ductility from other nanocrystalline materials, where abnormal grain growth is often observed. For example, after heating to a moderate temperature nanocrystalline nickel was reported to exhibit a bimodal microstructure and pronounced strain hardening under certain deformation conditions[25–27]. In addition to achieving a combination of strength and ductility, our thermomechanical approach to the processing of bulk samples is also simpler than those processes required to produce uniform nanocrystalline grains; the latter processes are not only difficult or expensive to implement, but also are difficult to keep free of artefacts such as porosity and impurities. In fact, fracture due to sample flaws after consolidation or deposition[2–4], together with plastic flow instabilities such as necking and shear banding[28], are responsible for the very limited strain to failure observed so far in nanocrystalline materials. □

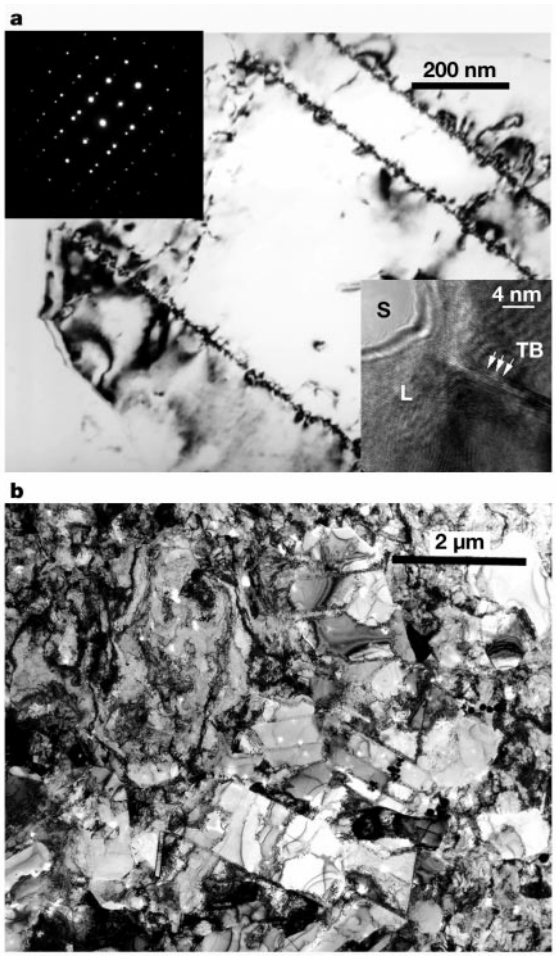

Figure 4 Transmission electron micrographs of Cu after different tensile strains. The Cu sample is that shown in Fig. 3b. **a**, after 6% plastic strain; the upper left inset shows the selected-area electron diffraction pattern, and the lower right inset shows the high-resolution image of the boundary region between a larger, micrometre-sized grain (L) and one of the surrounding much smaller ultrafine grains (S). A twin boundary (TB) is seen near the 'tip' of the S protrusion into L, where twinning is initiated. **b**, After the maximum uniform strain of ~30%.

Methods

Pure Cu (99.99%) bar from a commercial source (ESPI) was first processed by severe cold rolling, with liquid-nitrogen-temperature (LNT) cooling of the workpiece between consecutive rolling passes (−150 °C and −100 °C before and after each pass, respectively). The degree of LNT deformation is defined using per cent cold work[29], $\%CW = (S_o - S)/S_o \times 100\%$, where S_o and S are the cross-sectional areas before and after rolling. Some samples were processed through eight passes of equal channel angular pressing (ECAP) at room temperature before rolling, while others were subjected directly to LNT rolling. The ECAP step made no obvious difference to the eventual microstructure and properties, as the very large cold work energy stored at LNT controls the subsequent recrystallization behaviour. Microhardness, as well as the recrystallization temperature and enthalpy storage measured in a calorimetric scan, levels off after about 90% CW.

For mechanical property measurements, all the samples were cut and polished to a cross-section of 1 mm × 1.8 mm, and a gauge length of 5 mm (previously reported tensile tests of nanostructured metals typically used a gauge length in the range of 1–5 mm; refs 2, 5, 6, 25, 26). Uniaxial tensile tests were conducted at room temperature at an initial quasi-static strain rate of $5 \times 10^{-4}\ s^{-1}$.

Received 23 April; accepted 12 September 2002; doi:10.1038/nature01133.

1. Koch, C. C., Morris, D. G., Lu, K. & Inoue, A. Ductility of nanostructured materials. *Mater. Res. Soc. Bull.* **24,** 54–58 (1999).
2. Weertman, J. R. *et al.* Structure and mechanical behavior of bulk nanocrystalline materials. *Mater. Res. Soc. Bull.* **24,** 44–50 (1999).
3. Sanders, P. G., Youngdahl, C. J. & Weertman, J. R. The strength of nanocrystalline metals with and without flaws. *Mater. Sci. Eng. A* **234–236,** 77–82 (1997).
4. Sanders, P. G., Eastman, J. A. & Weertman, J. R. Elastic and tensile behavior of nanocrystalline copper and palladium. *Acta Mater.* **45,** 4019–4025 (1997).
5. Lergos, M., Elliott, B. R., Rittner, M. N., Weertman, J. R. & Hemker, K. J. Microsample tensile testing of nanocrystalline metals. *Phil. Mag. A* **80,** 1017–1026 (2000).
6. Valiev, R. Z., Alexandrov, I. V., Zhu, Y. T. & Lowe, T. C. Paradox of strength and ductility in metals processed by severe plastic deformation. *J. Mater. Res.* **17,** 5–8 (2002).
7. Gertsman, V. Y., Valiev, R. Z., Akhmadeev, N. A. & Mishin, O. V. Deformation behavior of ultrafine-grained materials. *Mater. Sci. Forum* **225–227,** 739–744 (1996).
8. Asgari, S., El-Danaf, E., Kalidindi, S. R. & Doherty, R. D. Strain hardening regimes and microstructural evolution during large strain compression of low stacking fault energy fcc alloys that form deformation twins. *Metall. Mater. Trans. A* **28,** 1781–1795 (1997).
9. Andrade, U., Meyers, M. A., Vecchio, K. S. & Chokshi, A. H. Dynamic recrystallization in high-strain, high-strain-rate plastic deformation of copper. *Acta Metall. Mater.* **42,** 3183–3195 (1994).
10. Youngdahl, C. J., Weertman, J. R., Hugo, R. C. & Kung, H. H. Deformation behavior in nanocrystalline copper. *Scripta Mater.* **44,** 1475–1478 (2001).
11. Gao, H., Huang, Y., Nix, W. D. & Hutchinson, J. W. Mechanism-based strain gradient plasticity-I. Theory. *J. Mech. Phys. Solids* **47,** 1239–1263 (1999).
12. Lu, L., Wang, L. B., Ding, B. Z. & Lu, K. High-tensile ductility in nanocrystalline copper. *J. Mater. Res.* **15,** 270–273 (2000).
13. Hughes, D. A. & Hansen, N. High angle boundaries formed by grain subdivision mechanisms. *Acta Mater.* **45,** 3871–3886 (1997).
14. Wang, Y. M., Ma, E. & Chen, M. W. Enhanced tensile ductility and toughness in nanostructured Cu. *Appl. Phys. Lett.* **80,** 2395–2397 (2002).
15. Humphreys, F. J. & Hatherly, M. *Recrystallization and Related Annealing Phenomena*, 1st edn 314 (Pergamon, New York, 1995).
16. Hertzberg, R. W. *Deformation and Fracture Mechanics of Engineering Materials*, 3rd edn 89, 392 (Wiley and Sons, New York, 1989).
17. Hart, E. W. Theory of the tensile test. *Acta Metall.* **15,** 351–355 (1967).
18. Dieter, G. E. *Mechanical Metallurgy*, 3rd edn 290 (McGraw-Hill, Boston, 1986).
19. Jia, D. *et al.* Deformation behavior and plastic instabilities in ultrafine-grained Ti. *Appl. Phys. Lett.* **79,** 611–613 (2001).
20. Wang, Y. M. & Ma, E. Strain hardening, strain rate sensitivity, and ductility of nanoconstructed metals. *Mater. Sci. Eng. A* (in the press).
21. Valiev, R. Z., Islamgaliev, R. K. & Alexandrov, I. V. Bulk nanostructured materials from severe plastic deformation. *Prog. Mater. Sci.* **45,** 103–189 (2000).
22. Huang, J. Y., Wu, Y. K. & Ye, H. Q. Deformation structures in ball milled copper. *Acta Mater.* **44,** 1211–1221 (1996).
23. Blewitt, T. H., Coltman, R. R. & Redman, J. K. Low-temperature deformation of copper single crystals. *J. Appl. Phys.* **28,** 651–660 (1957).
24. Lu, L., Sui, M. L. & Lu, K. Superplastic extensibility of nanocrystalline copper at room temperature. *Science* **287,** 1463–1465 (2000).
25. McFadden, S. X., Mishra, R. S., Valiev, R. Z., Zhilyaev, A. P. & Mukerjee, A. K. Low-temperature superplasticity in nanostructured nickel and metal alloys. *Nature* **398,** 684–686 (1999).
26. McFadden, S. X., Zhilyaev, A. P., Mishra, R. S. & Mukerjee, A. K. Observation of low-temperature superplasticity in electroplated ultrafine grained nickel. *Mater. Lett.* **45,** 345–349 (2000).
27. Hibbard, G. D., McCrea, J. L., Palumbo, G., Aust, K. T. & Erb, U. An initial analysis of mechanisms leading to late stage abnormal grain growth in nanocrystalline Ni. *Scripta Mater.* **47,** 83–87 (2002).
28. Wei, Q. M., Jia, D., Ramesh, K. T. & Ma, E. Evolution and microstructure of shear bands in nanostructured Fe. *Appl. Phys. Lett.* **81,** 1240–1242 (2002).
29. Callister, W. D. Jr. *Materials Science and Engineering*, 3rd edn 167 (Wiley and Sons, New York, 1994).

Supplementary Information accompanies the paper on *Nature*'s website (http://www.nature.com/nature).

Acknowledgements We thank G. Xu, H. Gao, S. X. Mao and D. van Heerden for discussions. This work was supported by the US National Science Foundation.

Competing interests statement The authors declare that they have no competing financial interests.

Correspondence and requests for materials should be addressed to E.M. (e-mail: ema@jhu.edu).

Variable effects of nitrogen additions on the stability and turnover of soil carbon

Jason C. Neff*†, Alan R. Townsend†‡§, Gerd Gleixner||, Scott J. Lehman§, Jocelyn Turnbull§ & William D. Bowman‡

** Earth Surface Processes Team, Geologic Division, US Geological Survey, MS 980, Denver Federal Center, Denver, Colorado 80225, USA*
‡ Environmental, Population and Organismic Biology; and § Institute for Arctic and Alpine Research, University of Colorado at Boulder, Boulder, Colorado 80309, USA
|| Max Planck Institute for Biogeochemistry, Jena, Germany
† These authors contributed equally to this work

Soils contain the largest near-surface reservoir of terrestrial carbon[1] and so knowledge of the factors controlling soil carbon storage and turnover is essential for understanding the changing global carbon cycle. The influence of climate on decomposition of soil carbon has been well documented[2,3], but there remains considerable uncertainty in the potential response of soil carbon dynamics to the rapid global increase in reactive nitrogen (coming largely from agricultural fertilizers and fossil fuel combustion). Here, using ^{14}C, ^{13}C and compound-specific analyses of soil carbon from long-term nitrogen fertilization plots, we show that nitrogen additions significantly accelerate decomposition of light soil carbon fractions (with decadal turnover times) while further stabilizing soil carbon compounds in heavier, mineral-associated fractions (with multidecadal to century lifetimes). Despite these changes in the dynamics of different soil pools, we observed no significant changes in bulk soil carbon, highlighting a limitation inherent to the still widely used single-pool approach to investigating soil carbon responses to changing environmental conditions. It remains to be seen if the effects observed here—caused by relatively high, short-term fertilizer additions—are similar to those arising from lower, long-term additions of nitrogen to natural ecosystems from atmospheric deposition, but our results suggest nonetheless that current models of terrestrial carbon cycling do not contain the mechanisms needed to capture the complex relationship between nitrogen availability and soil carbon storage.

Human activity now fixes more atmospheric N_2 into biologically available forms each year than all natural processes combined[4], causing a wide range of cascading environmental responses, including a possible sink for excess atmospheric CO_2 through stimulation of plant growth in N-limited ecosystems[5]. However, on average, soils contain three times as much C as does terrestrial vegetation[1]. Thus if changes in N availability alter soil C turnover, net C sinks from increased plant growth could be significantly enhanced or reduced, depending on the direction of the soil responses. Unfortunately, considerable uncertainty remains concerning the relationship between N availability and decomposition processes. Additions of N and/or natural variation in N concentrations have led to increases, decreases or no change in observed decomposition rates. This is true for field studies of litter and soil organic matter (SOM) decomposition, as well as for laboratory experiments[6–10].

In part, these varied results occur because decomposition studies are difficult to carry out and interpret. Soils are highly complex media with a diversity of substrates that vary in both the energy required for their breakdown and in their total N content. As a result, additions of N to soils could increase decomposition rates of some SOM fractions while simultaneously decreasing rates for other fractions. Past results suggesting widely varied—or no—responses of decomposition to N inputs may be due to varied and compensatory responses of SOM fractions that are difficult to detect with traditional measurements, such as mass loss or CO_2 efflux.

Data from long-term N-fertilized plots (defined as +N hereafter) at an alpine site on Niwot Ridge, Colorado, provide an example of the uncertainties associated with traditional measurements. Fertilized plots in dry meadow communities of alpine tundra at this site have received annual inputs of $10\,g\,N\,m^{-2}\,yr^{-1}$ since 1990 (ref. 11) (see Methods section). The decade of N fertilization has greatly increased productivity; over the past ten years, an average of $72\,g\,m^{-2}\,yr^{-1}$ of extra C has entered the fertilized plots (Table 1). Despite these increases in productivity, soil C concentrations are not significantly different between control and +N plots (Table 1). Against the large standing pools of SOM carbon on Niwot Ridge and elsewhere, large changes in C inputs or alteration of turnover times rarely result in statistically significant changes in soil C concentrations[12,13].

In contrast to bulk C values, the results of radiocarbon, ^{13}C and compound-specific analyses of soil C on Niwot Ridge all point to an acceleration of intermediate-age SOM turnover, and a possible increase in the stabilization of some forms of C into mineral SOM pools. Atmospheric testing of atomic weapons in the early 1950s led to a rapid increase in the ^{14}C content of atmospheric CO_2, followed by a gradual decline to the present[14] (Fig. 1). The time-dependent change in $^{14}CO_2$ can be used to examine the turnover time of intermediate-age soil C formed in equilibrium with the atmosphere. For soil samples, we performed ^{14}C measurements on 'light' and 'heavy' SOM fractions using a high-density solution. The heavy fraction is thought to be largely recalcitrant C associated with soil minerals, with turnover times of several decades to centuries, while the more labile light fraction reflects a mixture of compounds that includes microbial biomass, partially degraded plant material and older, more humified, by-products of decomposition[15,16]. In the dry meadow communities on Niwot Ridge, the light fraction is not significantly altered by fertilization and contributes over half of total soil C to both control and +N plots (Table 1).

The $\Delta^{14}C$ of incoming plant C determined from summer plant harvests from 1990 to the present is similar to the $\Delta^{14}C$ of

Table 1 **Productivity and soil C and N concentrations on Niwot Ridge**

	Above ground productivity ($g\,m^{-2}\,yr^{-1}$)	%C	Soil C in the light fraction (%)	%N	C:N ratio
Control	151 (11)*	8.61 (1.12)*	55.12 (2.14)*	0.67 (0.07)*	12.65 (0.74)*
+N	223 (16)†	10.40 (1.24)*	60.44 (1.91)*	0.83 (0.08)*	12.37 (0.33)*

Values shown are means with standard errors in parentheses. Statistically significant differences below the $P < 0.05$ level are shown by contrasting symbols within columns. Average annual productivity in the control and fertilized plots is significantly different ($F = 54.54$, $P < 0.001$). +N, long term N-fertilized plots.